




How vertical oscillatory motion above a saturated sand bed leads to heap formationK. Laurent ¹, L. La Ragione ², James T. Jenkins ³ and Gregory P. Bewley¹¹*Sibley School of Mechanical and Aerospace Engineering, Cornell University, Ithaca, New York 14853, USA*²*Dipartimento di Scienze dell'Ingegneria Civile e dell'Architettura, Politecnico di Bari, 70125 Bari, Italy*³*School of Civil and Environmental Engineering, Cornell University, Ithaca, New York 14853, USA*

(Received 11 March 2021; accepted 17 April 2022; published 5 May 2022)

We show how oscillations in fluid flow over a fluid-saturated and porous sediment bed leads to the development of a bedform. To understand the role of pressure fluctuations on the bed associated with flow oscillations, we analyze how the flow penetrates into and through the bed. We then calculate the corresponding vertical pressure gradients within the bed that tend to expand the bed along the vertical direction. When these pressure gradients are large enough, they facilitate small irreversible rearrangements of the grains within the bed, and so cause granular creep. We conjecture that this granular creep alternates with jamming to produce a granular ratchet that slowly lifts the surface of the bed locally where pressure gradients dominate, and depresses the surface where shear stresses dominate. We observe that the shape of the resulting heap exhibits a constant characteristic width. The height of this heap evolves approximately as the square root of time, in agreement with dimensional arguments predicated on a coarse-grained viscous deformation of the bed. The surface of the heap contracts initially with the square root of time, consistent with an incompressible analysis of the flow of grains within the heap. Near its peak the heap grows due to a dilatation of the bed, to inward radial flux, or to a combination of the two.

DOI: [10.1103/PhysRevE.105.054901](https://doi.org/10.1103/PhysRevE.105.054901)**I. INTRODUCTION**

Initially flat granular beds are unstable under many conditions, and give rise to various types of bedforms including ripples, dunes, and antidunes [1]. These bedforms are responsible for the shape and evolution of terrains including deserts [2], seabeds [3], and the surfaces of other rocky planets, such as Mars and Venus [4,5]. Bedforms protect against damage caused by natural disasters such as hurricanes [6], but can also themselves be dangerous by causing sandslides [7] and unsafe shoal waters [8].

The size, shape, and spacing of bedforms depend on flow characteristics, such as velocity and flow depth, as well as sediment characteristics, such as size and grading [9–11]. In order to predict the development and erosion of bedforms, it is necessary to understand the particle-fluid interactions within granular beds, as has been done in various geometries including tumblers, shakers, and flumes [9,12,13]. Due in part to large variations in the grain properties and fluid environments, it is both a challenge and an opportunity to identify mechanisms and formulate scaling laws that describe the dynamics of the coupled particles and fluid.

Bedforms generally arise in turbulent environments, and the forces imposed on the bed by the surrounding fluid flows cause sediment beds to become unstable sooner than predicted by canonical shear-driven models [14–16]. Both mean flows and turbulent fluctuations impose shear stresses on beds, and understanding the effects of these stresses is an ongoing challenge [17,18]. Pressure fluctuations can be associated with surface waves [19,20], internal waves [21], or turbulence.

When vertical forces caused by the pressure gradients are large enough, they expand a bed and cause its failure grains to become mobile. We show that the recurrence of these large vertical forces leads to the development of bedforms.

Traditional sediment transport theories operate under the assumption that transport depends only on the mean shear stress at the bed [2,22]. However, experiments on the effects of pressure fluctuations caused by turbulence show that single particles experience fluctuating lift forces due to pressure differences between the top and the bottom of the particles [23,24]. Foster *et al.* [25] observed that horizontal pressure gradients influence the onset of sediment motion. Models incorporating this additional force generate more accurate predictions [26], especially in cases where turbulence is dominant and mean shearing is minimal, such as in the swash zone [27].

Recently, Johnson [14] observed sediment transport in turbulent flows absent of mean flow-induced shear. She performed experiments using randomly actuated jets to develop homogeneous isotropic turbulence with no mean flow above a flat bed of sand. Over the course of a couple of hours, prominent ripples developed in the sand bed. The researcher noted that there existed a linear relationship between the ripple spacing and the integral length scale of the turbulence but were unable to fully explain the development of the ripples. She hypothesized that the appearance of the ripples may be due to pressure fluctuations above or within the sand bed.

Seepage may have an effect on pressure gradients imposed on grains below the bed's surface, which in turn affects the development of bedforms and the transport of moisture and

dust. Comparisons between the pressure fluctuations imposed on solid [28] and porous [29] surfaces show that porosity can affect the surface pressure gradients and induce a slip velocity. Though sediment transport models traditionally consider only shear forces experienced by surface grains [2,22], Louge *et al.* [30] suggest that seepage-induced body forces may result in a lowered threshold for sediment transport than the threshold predicted by these models.

The goal of this work is to contribute to an understanding of the onset of sediment motion due to pressure gradients. In Ref. [31], we showed that a granular bed under an oscillating plate forms a heap, similar to those observed in vibrated granular beds [13,32,33]. The oscillating flow, generated by the plate motion, induced pressure gradients at the surface and in the interior of the bed. In this paper, we extend the theory and data analysis to capture the evolution of the heap. The upward motion of the plate draws fluid up through the center of the bed and lifts a layer of beads, permitting small reconfigurations of the bed with every cycle of the plate motion. We find that the development of the heap is approximately self-similar in time and can be explained with simple scaling arguments. For instance, the heap height increases approximately as the square root of time. As a consequence of mass conservation, the surface of the heap contracts at a similar rate. The rate of contraction, however, is modified by a factor determined by the shape of the heap.

II. EXPERIMENT

We performed the experiments in a 50-cm-long and 30-cm-wide glass tank, which we filled with glass beads to a depth of 8 cm. The glass beads had a mean diameter, d , of 0.5 mm, an approximately uniform size distribution between 0.43 and 0.60 mm, and a mass density of 2.5 g/cm^3 (Potters Industries, P-0230). After filling the tank with beads, we filled the tank with water to 8 cm above the bed of glass beads. A schematic of the apparatus can be seen in Fig. 1.

A cross beam held an electromagnetic shaker over the tank. Attached to the shaker was a 7.5 cm square plate, which was horizontally centered in the tank and oscillated up and down under the water. We observed the development of heaps in the bed over a period of hours, corresponding to plate oscillations ranging from $O(10^4)$ to $O(10^5)$ in number. We performed the experiment for plate oscillation frequencies, f , between 10 and 40 Hz, amplitudes, A , between 0.02 and 0.14 cm, and at a fixed mean height above the bed, H , of 2.7 cm.

We measured the height profiles of heaps with a red laser sheet produced by reflecting a laser beam off of a cylindrical surface. The laser sheet illuminated the surface of the bed of glass beads, producing a bright curve in images of the heap taken from the side. Before each experiment, we used an acrylic sheet to flatten the bed. This initial condition is illustrated in Fig. 1 (top left) and we acquired a series of images at regular intervals as the heap developed in the bed, as seen in Fig. 1 (top right).

We determined the profile of the bed using an algorithm that followed the path with the highest red intensity in the images of the heap. We found the center of the heap by averaging the position associated with the maximum height

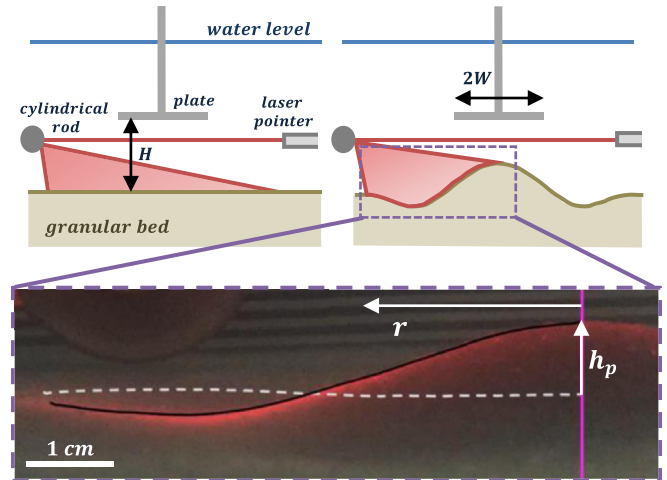


FIG. 1. Top left: A laser beam (red) reflected off a cylinder to form a vertical light sheet. A plate with width $2W$ oscillated about a mean height H above the bed. Before each experiment, we flattened the bed using an acrylic sheet. Top right: After many oscillations of the plate, a heap developed in the bed. By taking images at regular intervals in time, we quantified the evolution of the bed's shape. Bottom: In this image of the heap from the side, the surface of the heap is marked with a black curve determined using an algorithm. The initial bed height is marked with a dashed white curve and the centerline with a vertical purple line. We measured the radial distance, r , as the horizontal distance from the centerline.

of the heap and taking the median value of that position in the latter half of the time-lapse videos. The results of this method can be seen in Fig. 1 (bottom), where the dashed line indicates the initial configuration of the bed, the solid black line indicates the measured surface of the bed as determined by the technique described above, and the purple line indicates the center of the heap. Note that, although we leveled the bed with an acrylic sheet before each experiment, the bed was not completely flat and the initial height varied slightly.

To measure the amplitude of the plate oscillations, we took slow-motion videos of the plate and found the positions of the plate by placing a black dot on the edge of the plate and tracking the dot. To convert the size of the heap and plate oscillations from pixels to millimeters, we placed a ruler in the tank and aligned it with the laser sheet and to the near side of the plate. We used images of the ruler to calibrate the ratio between image pixels and the millimeter markers on the ruler.

In order to track the motion of grains on the surface of the bed in the horizontal direction, we placed black beads on the surface and took pictures of the bed every 10 min. Figure 2 shows a ring of such beads initially, after 20 min of plate oscillations, and after 60 min of plate oscillations. To take images from above the heap, we stopped the experiment, removed the plate, took the image, replaced the plate, then restarted the experiment, taking care to disturb the bed as little as possible during the process. We measured the radius of rings of beads on the surface as functions of time by fitting ellipses to the minima in the intensity of images of the rings taken at regular intervals. Since the rings were not exactly

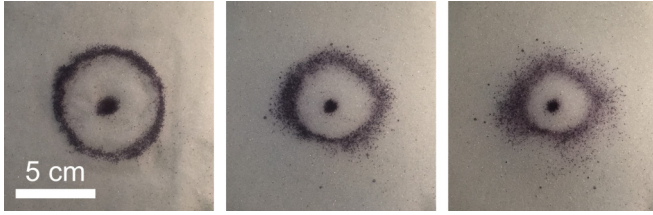


FIG. 2. Images taken from directly above the bed at different times increasing from left to right. A ring of dark beads on the surface of the bed drew in toward the center over time. A spot of dark beads in the center stayed in the center while also contracting slightly. In both cases the beads stayed at the surface of the bed. The left-most image is of the bed in its initial flat condition, and the subsequent images were taken 20 and 60 min after being subjected to oscillations of the plate at a frequency of 20 Hz and an amplitude of 0.4 mm.

circular, we tracked both the major and minor axes of the ellipses.

III. THEORY

On the sediment bed in the experiment, shear stresses under the periphery of the plate give way to normal stresses beneath the center of the plate. Ignoring normal stresses, the importance of mean shear stresses to the stability of the bed is embodied in the Shields parameter, $\theta = \tau / \Delta \rho g d$, which makes the shear stress, τ , dimensionless with the density difference between the sediment and fluid, $\Delta \rho = \rho_s - \rho$, gravitational acceleration, g , and the sediment grain diameter, d [22,34]. In order to suggest a corresponding parameter, which we call ϕ , with which to gauge the importance of normal stresses, we examine the balance of forces on grains within the bed. We suggest that the pair θ and ϕ are then the dimensionless parameters that describe the conditions in the experiment.

In Sec. III A, we analyze the instability mechanism introduced by La Ragione *et al.* [31]. We elaborate on the mechanism and show how the onset of sediment motion results when fluid flows generate vertical pressure gradients within the bed large enough to lift part of the bed directly. In this section, we introduce a parameter $\phi = (Uf/g)(\rho/\Delta\rho)$ that measures the importance of normal stresses, and we propose that sediment motion occurs for $\phi \gtrsim c/26.4$. In Sec. III B, we examine the subsequent evolution caused by this instability of an initially flat bed into a heap, and do so in the context of a continuum model, which has been utilized in other granular applications [35–38], that captures the essential features of the heap’s evolution.

A. Onset of heap formation

Given the symmetry in the experiment, radial bedload transport arising from shear stress on the bed at high Shields numbers would lead either to an accumulation at the center of material from the sides or to a pit, depending on the direction of mean transport. In the experiment we observed the former. Furthermore, we observed that beads on the surface of the bed remained on the surface during heap growth. Since the accumulation of material associated with bedload transport

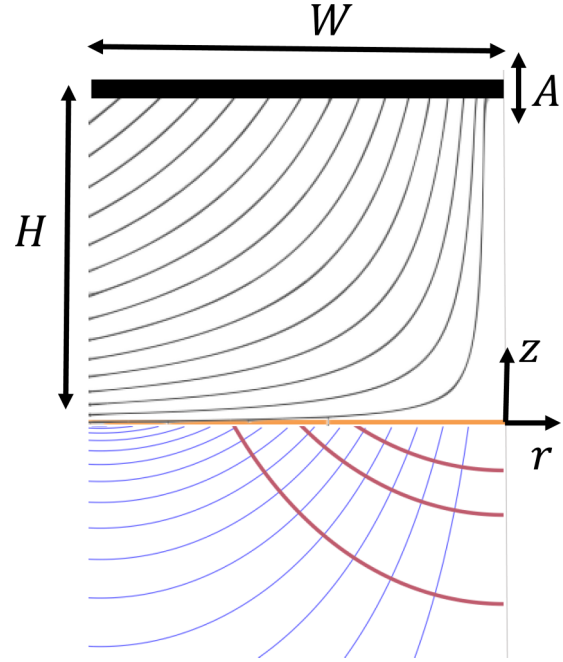


FIG. 3. Half of the oscillating plate appears as a horizontal bar at $z = H$. Its full width is $2W$ and it oscillated vertically with amplitude A . The curves between the plate at $z = H$ and the bed surface at $z = 0$ are the streamlines of an inviscid stagnation point flow. This flow applied an oscillating pressure on the surface of the bed, which in turn generated flow through the porous bed modeled by Darcy’s law and shown by the blue streamlines and red isolines of pressure. We predict sediment transport primarily under the origin of the coordinate system, and the peak of the observed heap grew up along the z axis at $x = 0$.

would tend to bury those beads in the center of the bed, we sought a different explanation for the sediment motion. While bedload transport may play a role in the observed heap development, particularly around the margins of the heap, we concentrated on prediction of possibly more novel aspects, which include the lifting of beads near the surface of the heap. In the following, we focus our analysis on vertical pressure gradients near the axis of symmetry of the heap, and continue our description of the flow away from this axis only as needed to provide boundary conditions consistent with basic physics such as mass conservation.

We idealize the experiment as an axisymmetric oscillatory flow of an incompressible fluid driven by vertical oscillations of a horizontal bar (or plate) above a flat porous bed, as shown in Fig. 3. We note the remarkable azimuthal symmetry of the heap observed in the experiments despite the square shape of the plate (e.g., Fig. 2). That is, the flow of the fluid and deformation of the bed seemed unaffected at the leading order by the particulars of the geometry.

We divide the flow into two parts: one above the bed and one within the bed. Above the bed, we approximate the flow generated by the oscillating plate as the one near an inviscid stagnation point whose amplitude varies sinusoidally in time at a given frequency, f . We specify this flow over the bed in order to set the boundary condition for the flow through the bed, which is the pressure distribution on the surface of

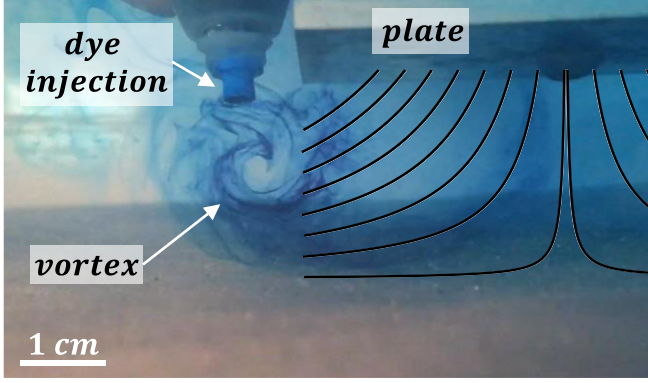


FIG. 4. Blue dye injected into the flow generated by plate oscillations showed a region beneath the plate within which the dye followed the streamlines (black curves) of an inviscid flow associated with a stagnation point. These streamlines are superimposed on the image. In the inviscid theory, the fluid motion is symmetric in time and so flows in both directions along the streamlines. In the experiment and outside the boundary of the plate, the flow curled into a slow clockwise vortex whose turnover time was much longer than the period of plate oscillations. Our analysis of the effects of fluid motion on the bed applies to the region directly under the plate.

the bed. Within the bed, which is porous, the fluid motion continues as a linear viscous flow according to Darcy's law.

In order to calculate the pressure distribution on the surface of the bed, we first consider the flow above the bed. The equations that govern the motion of the fluid are the balances of mass and momentum [39]. As a first approximation, we consider an inviscid fluid because the plate Reynolds number is large ($\text{Re} = AfW/\nu$ is about 10^2), and we linearize the dynamics because the fluctuations are small. These approximations do not hold near the edge of the plate, where a shear layer and vortex typically develops, or at the surface of the bed, where a boundary layer forms. The vortex we observed (see Fig. 4) was confined to the region outside of the plate boundaries, so that our approximations are more realistic under the plate and where we predict bed instability. We neglect the viscous boundary layer on the surface of the bed because pressure is approximately constant across the thickness of boundary layers.

The amplitude of the oscillations, A , is small compared with the mean height of the plate above the bed, H . Under static conditions, the pressure is $p_0 = -\rho g(H - z)$, where g is the gravitational acceleration. The fluid's radial velocity is $u(r, z, t)$, its vertical velocity is $v(r, z, t)$, the fluid pressure is $p(r, z, t)$, and its constant mass density is ρ . In the fluid above the bed (for $0 \leq r \leq W$ and $0 \leq z \leq H$), the system of equations governing the problem are

$$\frac{1}{r} \frac{\partial(ru)}{\partial r} + \frac{\partial v}{\partial z} = 0, \quad (1)$$

$$\rho \frac{\partial u}{\partial t} = -\frac{\partial p'}{\partial r}, \quad \text{and} \quad (2)$$

$$\rho \frac{\partial v}{\partial t} = -\frac{\partial p'}{\partial z}, \quad (3)$$

for conservation of mass, radial momentum, and vertical momentum, respectively, where the prime indicates a deviation

from hydrostatic conditions. Terms proportional to viscosity are absent, since we assumed inviscid flow.

In order to estimate the variation of the pressure in space and time, we separate the space and time dependencies of the flow. Under the plate (for $0 < r < W$ and $0 < z < H$), we specify that the radial and vertical components of the flow velocity are $u(r, z, t) = k(t)r/2$ and $v(r, z, t) = -k(t)z$, where $k(t)$ sets the strength of the flow and the way it varies in time.

Under the plate (for $0 < r < W$ and $0 < z < H$), Eqs. (2) and (3) in combination with the stagnation point flow introduced above give

$$\frac{1}{2}\rho r \frac{dk}{dt} = -\frac{\partial p'}{\partial r}$$

and

$$\rho z \frac{dk}{dt} = \frac{\partial p'}{\partial z}.$$

The solution for the pressure given by these equations is

$$p' = -\frac{\rho}{4} \frac{dk}{dt} (r^2 - 2z^2 - W^2), \quad (4)$$

where the constant of integration is found by observing that on the bed ($z = 0$) the pressure induced by the plate motion decays away from the center of the plate, and by prescribing that at $r = W$, the induced pressure is zero.

Then, at the bed, the pressure induced by the plate through the fluid is

$$p'(r, 0, t) = \frac{\rho}{4} \frac{dk}{dt} (W^2 - r^2). \quad (5)$$

The oscillatory motion of the plate in the experiment is an approximately sinusoidal function in time. The vertical fluid velocity at the plate, the time derivative of its position, is given by $v' = (2\pi f)A \cos(2\pi ft)$, where A is the amplitude of the plate's oscillations and f is the frequency of oscillation. We combine this expression for v with the vertical velocity of an inviscid stagnation point flow, $v = -k(t)z$, and find at $z = H$ that

$$(2\pi f)A \cos(2\pi ft) = -Hk(t). \quad (6)$$

From this equation, we find an expression for the time derivative of k and substitute this derivative into Eq. (5). The pressure on the bed in excess of hydrostatic contributions is then

$$p'(r, 0, t) = -\frac{\rho}{4} \frac{A}{H} (2\pi f)^2 \sin(2\pi ft) (r^2 - W^2), \quad (7)$$

with $0 < r < W$.

We now turn to the flow within the porous bed, which we describe with a linear continuum model. Within the bed (for $z < 0$ and $0 \leq r \leq W$), the mass balance is

$$\frac{1}{r} \frac{\partial r q_r}{\partial r} + \frac{\partial q_z}{\partial z} = 0, \quad (8)$$

where $q_r = (1 - c)u$, $q_z = (1 - c)v$, u and v are coarse-grained interstitial fluid velocities, and c is the volume fraction of particles in the bed, which we assume is constant. Ignoring the compressibility and inertia of the fluid, we follow Darcy's

law [40], which states that

$$-\frac{\partial p'}{\partial r} - \frac{\mu}{\kappa} q_r = 0 \quad (9)$$

and

$$-\frac{\partial p'}{\partial z} - \rho g - \frac{\mu}{\kappa} q_z = 0, \quad (10)$$

where κ is the permeability of the bed and μ is the viscosity of the fluid. Under this hypothesis, the flow has no internal timescales and it evolves quasistatically with a velocity proportional to the instantaneous gradient in pressure. By substituting Eqs. (9) and (10) into Eq. (8), we find that mass conservation is described by the Laplace equation,

$$\frac{1}{r} \frac{\partial}{\partial r} \left(r \frac{\partial p'}{\partial r} \right) + \frac{\partial^2 p'}{\partial z^2} = 0, \quad (11)$$

which conveniently eliminates the constants that characterize the bed and fluid, under the assumption that their spatial gradients are zero.

The flat bed becomes unstable when vertical pressure gradients within the bed exceed the buoyant weight of the bed. To calculate this critical pressure gradient, we solve Eq. (11) with the boundary conditions given (in part) by Eq. (7) (see the Appendix). The solution for the perturbations to the pressure in the porous bed is

$$p'(r, z, t) = 0.28 \rho \frac{A}{H} (\omega W)^2 \times e^{2.41z/W} J_0(2.41r/W) \sin \omega t, \quad (12)$$

and is characterized by an exponential decay into the bed in which J_0 is the Bessel function of the first kind. This fast decay of the flow below the surface is consistent with the observation reported by La Ragione *et al.* [31] in that placing a flexible circular cylinder in the bed, blocking the flow beneath the bed, prevented the development of heaps only when the blockage extended to within ten bead diameters of the surface.

The maximum vertical gradient of the pressure given by Eq. (12), $\partial p'/\partial z|_{\max}$, is located at the origin and when the plate is at its maximum excursion from its mean position. Its particular value is given by

$$-\frac{\partial p'}{\partial z} \Big|_{\max} \doteq 2.41 \times 0.28 \rho \frac{A}{H} W \omega^2.$$

In the special case for which the plate is as far from the bed as its half width, or for $H = W$, which was approximately the condition in the experiment, the maximum gradient in pressure is further simplified and is

$$-\frac{\partial p'}{\partial z} \Big|_{\max} \doteq 26.4 \rho A f^2. \quad (13)$$

The difference between this critical pressure gradient and the one given by the full dynamic pressure applied across a sediment grain, $\rho(Af)^2/d$, is the (large) geometric factor of 26.4 when the plate moves by the diameter of a grain, which is due to the resistance of porous materials.

We balance the maximum induced pressure gradient with the buoyant weight of the bed, $(\rho_s - \rho)cg$, to determine the

following condition for instability of the flat bed:

$$Af^2|_{\text{failure}} = \frac{c}{26.4} \frac{\Delta \rho}{\rho} g, \quad (14)$$

where $\Delta \rho = \rho_s - \rho$. This equation describes a limit above which particles in the bed will be lifted by the flow.

We reexpress the criterion in Eq. (14) as a parameter, ϕ , that makes pressure dimensionless in the same way that the Shields parameter makes the shear stress dimensionless. We define ϕ by rearranging Eq. (14), and by noting that $U = Af$ is a characteristic (vertical) velocity, so that

$$\phi \equiv \frac{Uf}{g} \frac{\rho}{\Delta \rho}, \quad (15)$$

which compares flow accelerations with gravitational acceleration reduced by buoyancy. Because the particle volume fraction, c , does not change substantially over time or between different compact beds, we ignore it in the definition of ϕ . When pressure gradients dominate gravity, we expect the flat bed to be unstable for large values of ϕ . For a random close packing of spheres, $c_{\text{RCP}} \approx 0.64$ [41]. Using Eq. (14), we estimate that the onset of this instability occurs when $\phi_{\text{RCP}} = c_{\text{RCP}}/26.4 \approx 0.024$.

B. Bed evolution

Once a flat bed becomes unstable as described in the previous section, and continues to evolve periodically as the flow through it oscillates, we need to explain the subsequent slow uplift of the bed into a heap. We conjecture that the bed reshapes itself by creeping, or through small rearrangements of the grains within the heaping region of the bed. Unlike the creep analysis in previous studies that was driven by a mean shear [42], we suppose instead that oscillatory flow through the heap drives creep, especially near the vertical axis of symmetry. We also suppose that creep occurs primarily during upward flows, and that the bed locks into place, or jams, during downward flows [43–45]. This asymmetry with respect to time in the behavior of the bed enables the accumulation of a net deformation, and constitutes a kind of granular ratchet [46].

During upward motions of the plate, the particles of the heaping region of the bed are able to move; during downward motions, the particles are locked and the bed is rigid. The oscillations of the plate are far more rapid than the resulting deformation of the bed. Hence, the slow motion of the bed may be taken to be in response to the average flow of the fluid during the upward motion of the plate. In this case, the motion of the bed is forced by the fluid shear stress at its surface and forces associated with gradients of the fluid pressure in its interior.

The size of the fluid shear stress at the bed surface may be estimated using the boundary layer analysis of Batchelor (see pp. 287–288 of [39]), with the x component of the steady velocity at the surface being proportional to $2\pi(A/H)fx$. The resulting shear stress is proportional to $(\rho\mu)^{1/2}(Af/H)^{3/2}x$. The stresses associated with the gradients of the fluid pressure in its interior are, roughly, the product of the pressure gradient in Eq. (13) and the extent, W , of the fluidized region: $\rho AW^2 f^2/H$. The ratio of the first to the second is on the

order of 10^{-3} , which indicates that the surface shear stresses may be ignored relative to the normal stresses induced by the fluid pressure gradients. This emphasizes the difference in bed formation in rapid oscillatory flows and those driven by superficial shear stresses alone.

To capture the essential response of the bed to the applied stresses, we suppose that the bed behaves as a linear viscoplastic granular flow [47,48]. That is, we assume that the slow deformation of the bed by the grain-scale processes outlined above can be described approximately as a coarse-grained viscous flow characterized by an effective kinematic viscosity, ν_g . The resulting predictions include how the height of the bed and the radius of a ring on its surface change in time, predictions that compare favorably with the data presented in Sec. IV.

We assume that the shape of the heap is invariant with time when scaled by a single length scale. This characterization may be reasonable for times much larger than the period of the flow oscillations and much smaller than the one required for the heap to grow large enough to modify the flow geometry. The characterization may fail for heaps containing too few grains, or heaps approaching the size of their container. That is, we seek an intermediate asymptotic description of the evolution of the bed in terms of a single length scale [49], which we take to be the height of the bed at the peak, h_p .

According to dimensional analysis [50], if a physically meaningful equation exists that relates h_p and t , then $h_p(t)$ must be proportional to $\sqrt{\nu_g t}$. We rewrite this proportionality in terms of the dimensionless heap height, $h_p(t)/d$, and the dimensionless time, tf , as follows:

$$\frac{h_p(t)}{d} = C_h (tf)^{1/2}, \quad (16)$$

where the dimensionless prefactor, $C_h(\text{Re}_g)$, is unknown but for proportionality to $\text{Re}_g^{-1/2}$, where $\text{Re}_g = d^2 f / \nu_g$ is a Reynolds number that arises due to our choice of dimensionless variables. Equation (16) constitutes our prediction for the temporal development of the heap.

Because the problem contains more dimensions than we included in our analysis, the dimensionless prefactor, C_h , is likely to contain additional dependencies that can generate exponents different from $1/2$ in principle. These additional dimensions include, for instance, the characteristic speed and length scales of the flow above the bed (Af and W), and the densities of the sediments and fluid. These additional dependencies appear to be negligible in the regime of our interest, where h_p is small compared with H and h_p/t is small compared with U , for instance, while other parameters likely did not vary appreciably in our experiments, including W/H and UW/ν_g . Future experiments are needed to develop a more detailed understanding of the mechanisms at play.

To see how a bead on the surface of the bed migrates during the growth of the heap, we describe the radial flow of sediments within the bed in a depth-averaged sense while ignoring diffusion of the grains. Consider that the change in heap height at any radius, r , is given in part by the flux into an annular control volume centered on r and in part by changes in the mass density of the bed. Granular beds are generally compressible; grains can rearrange themselves to occupy more or less volume. However, for simplicity, we initially assume an

incompressible flow of grains, though the data do not preclude contributions from changes in mass density, and we revisit this assumption below. For an incompressible bed, where changes in the depth-averaged radial flux, $\bar{u}T$, exactly balance changes in the height, h , we have

$$\frac{\partial h}{\partial t} = -\frac{T}{r} \frac{\partial(r\bar{u})}{\partial r}, \quad (17)$$

where $\bar{u}(r, t)$ is the mean radial velocity of beads moving in a surface layer with thickness $T(r, t)$.

Since the shape of the heap is approximately invariant with time, we can separate the time and space variations of the height, so that $h(r, t) = h_p(t) \alpha(r)$. According to the dimensional arguments summarized in Eq. (16), $h_p/d \sim (tf)^{1/2}$. We then solve for the mean radial bead velocities in the heap by integration of Eq. (17) over the radius. Given the boundary conditions, we find the depth-averaged radial velocity to be

$$\frac{\bar{u}(r, t)}{fd} = -\frac{1}{2} C_h \text{Re}_g^{-1/2} G(r, t) (tf)^{-1/2}, \quad (18)$$

with

$$G(r, t) = \frac{1}{r} \int_0^r \frac{\alpha(\xi)}{T(\xi, t)} \xi d\xi. \quad (19)$$

The dimensionless function G depends on the thickness of the layer of mobile beads, $T(r, t)$, which we did not measure, and on the shape function, $\alpha(r)$, which we did measure. Large G corresponds to tall heaps within which motion is confined to a thin layer. Assuming that T does not vanish at the peak, plausible assumptions about its shape, including that it is constant or determined by α itself, lead to qualitatively similar conclusions, namely, that the velocity of the ring approaches zero more quickly than $t^{-1/2}$ at small radii. This slowdown can give the appearance that superficial beads cease their mean radial motion entirely within a region near the axis, a notion we revisit below. We note an analogy between this analysis and the one of hydrogen particles on a quantized vortex ring in Ref. [51], in which an underlying square-root decay in time is modified by drag between the particles and fluid.

According to the arguments above, the radius, R , of a ring of beads on the surface of the heap is proportional to the square root of time far from the axis and when $n = 1/2$, since its radius changes as $dR = \bar{u}(R, t) dt$ and integration yields

$$1 - \frac{R}{R_0} \sim G(R) \frac{d}{R_0} (tf)^n, \quad (20)$$

where R_0 is the initial radius. At long times [49], a stable configuration of the heap is reached and it stops growing. Equations (16) and (20) constitute the two predictions that we compare with data in the next section.

IV. RESULTS AND DISCUSSION

We performed the experiment at various oscillation frequencies corresponding to a range of values for ϕ in Eq. (15) from 0.004 to 0.03. In natural flows, ϕ can be arbitrarily small and reaches values larger than 0.1 for turbulent flows under water. In the experiment and under the perimeter of the plate, we estimate the Shields parameter θ to be no larger than $O(10^{-3})$ in any of our experiments, which is smaller than

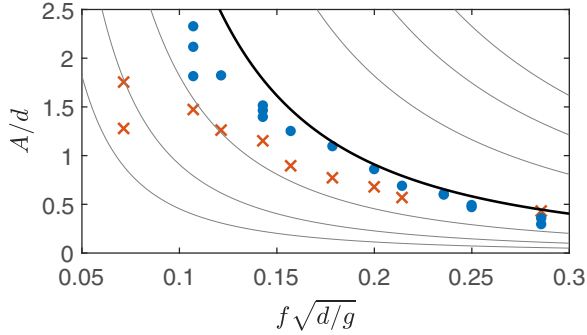


FIG. 5. Prediction of sediment motion by ϕ . Experimental data are represented by circles (blue) and crosses (red): circles when sediment motion occurred and crosses when it did not. The solid lines are curves of constant ϕ , defined in Eq. (15). The thickest line corresponds to the value $\phi_{\text{RCP}} = 0.024$. We find that $\phi \approx 0.020$ generally separates conditions that formed heaps from those that did not. Values above this one correspond to integer multiples of ϕ_{RCP} and those below to $1/2$, $1/4$, and $1/8$ of ϕ_{RCP} . Note that the predicted onset of sediment motion using the Shields theory [22] corresponds to A/d values of $O(1000)$.

the value ($\gtrsim 0.02$) observed for the onset of sediment motion under steady shear flow [22,52]. The Reynolds numbers of the plate, $\text{Re} = 2WAf/\nu$, ranged from approximately 500 to 1500.

A. Onset of heap formation

We review in this section the finding we reported in Ref. [31], which is that bedforms developed only under those conditions shown in Fig. 5. For lower amplitudes of the plate motion, no bedform developed. When the bedforms did develop, it took many oscillations of the plate to do so—on the order of hundreds of thousands. The heap resulted from the cumulative effect of many very small motions in the bed. The data are consistent with the onset of flat-bed instability being described by the theory in the previous section and by Eq. (15), that is, for large $\phi \sim Af^2$. The particular form of the curve of constant ϕ is distinctive of the onset of heap formation due to vertical pressure gradients and not shear stresses. The particular value of the critical ϕ_0 for the onset of heap formation determined from the experiment, $\phi_0 = 0.02$, compares favorably with the factor $c/26.4 \lesssim 0.03$ for packed spherical particles, as predicted by Eqs. (14) and (15).

B. Heap profile

The profiles of the bed, $h(r, t)$ in Fig. 6, show that after a few thousand cycles the shape of the heap was approximately invariant in time when appropriately rescaled. There was an initial transient during which the peak was flat and the annular trough around the heap was deep relative to later times. This initial heap development was sensitive to initial conditions; it was different in different experiments.

The profiles reported in Ref. [31] are reproduced in Fig. 6 (left), and replotted in Fig. 6 (right) normalized by their peak height at each time, $h_p(t)$, in order to evaluate the assumption that, upon rescaling of the heap, the shape of the heap does

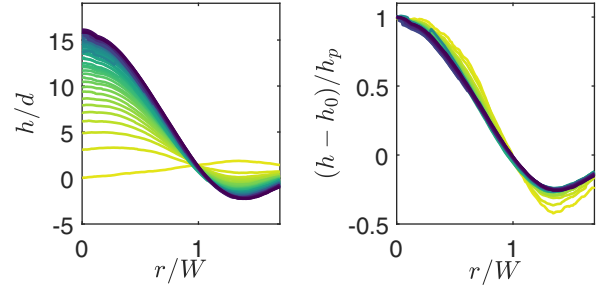


FIG. 6. Left: The profile of the bed, $h(r, t)$, at intervals of 4800 cycles (320 s), resulting from plate oscillations with an amplitude of $A/d = 2.72$. Color transitions from yellow to purple indicate increasing time. The profile is normalized by the diameter of the glass beads, d , and the radius is normalized by the plate half width, $W = 3.8$ cm. Right: The profile of the bed with respect to the initial height of the bed, $h_0(r) = h(r, 0)$. Each profile is normalized by its peak height, $h_p(t) = h(0, t)$. The profiles are approximately invariant in time after an initial transient. We call the invariant profile $\alpha(r/W)$. The inset shows all profiles, including h_0 , normalized by the bead diameter, d , and the radius normalized by the plate half width.

not change with time. As in Eq. (19), we call the shape that the heap approached $\alpha(r/W)$, whose form we know only from these measurements. Empirically, we found that the first zero crossing of the data was a constant equal to about 3.7 cm. Note that the radius at which no material accumulated is also, in principle, the radius at which there was a maximum in the radial flux of material across the bed.

C. Bed evolution

The heap height grew as shown in Fig. 7. Below a certain threshold oscillation amplitude near $A = 0.38$ mm at a frequency of $f = 15$ Hz, no heap formed. Above this threshold, the heap height data are consistent with a power law in time with an exponent of $1/2$, shown in Fig. 7 as black lines.

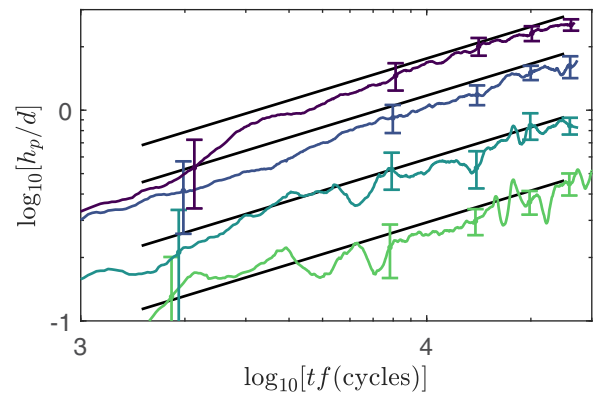


FIG. 7. The growth of the peak height, h_p , was consistent with the square root of time (black line) predicted in Eq. (16). From the lower to the upper curve, the normalized plate oscillation amplitudes were $A/d = 1.64$, 1.76 , 1.92 , and 2.04 . No heap grew for a normalized oscillation amplitude of less than 1.52. The normalized oscillation frequency for all cases was $f\sqrt{d/g} = 0.11$. The data are smoothed using a moving average and error bars indicate the standard error for a few select points.

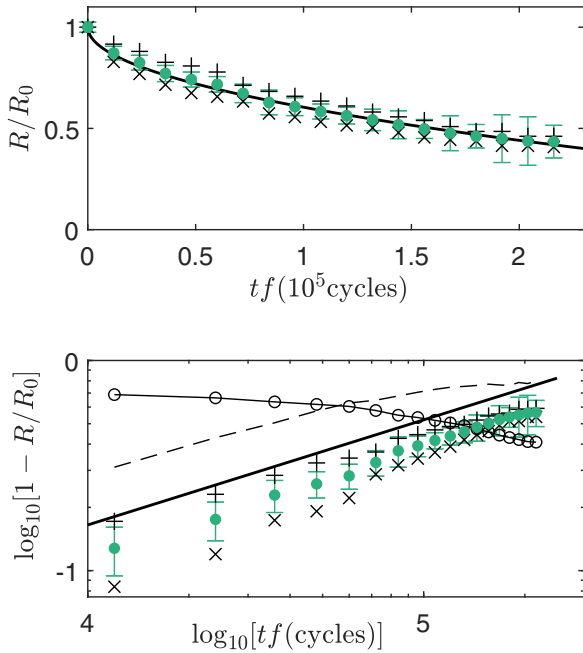


FIG. 8. Top: The radius of a ring, $R(t)$, on the surface of the heap contracted over time, shown by the major (\times) and minor ($+$) axes of an ellipse fit to images of the ring, their mean (\bullet), and a square-root function for reference ($-$). The square-root contraction goes hand-in-hand with the heap growth as described in the text. The initial radius was $R_0 = 2.8$ cm, and the frequency of the plate oscillations was $f = 20$ Hz. Bottom: The logarithmic scale reveals that as the ring approached the peak of the heap, its contraction slowed down relative to the square root of time. The product of the shape factor, $G(R)$ in Eq. (20) ($-o-$), and a $1/2$ power law shows that the combination of geometric effects with the slowing dynamics reproduces the observation that the ring radius reached an approximate constant at large times ($-$).

This exponent is consistent with Eq. (16). Note that beads deposited on top of the center of the heap stayed on the top of the heap as the heap rose upward, while remaining centered and contracting slightly in radius [31].

Figure 8 shows the radius of a ring on the surface of the heap as a function of time. Initially, the ring contracted approximately as the square root of time, in agreement with Eq. (20) for constant G . The ring contraction subsequently slowed down relative to a power law when it became small relative to its initial diameter. This slowdown is consistent with the behavior of $G(R(t))$, which is not constant as we now explore.

In order to understand the role of the shape factor, $G(R(t))$, and to illustrate its essential behavior, we fit a polynomial to the data in Fig. 6 and then integrated Eq. (19) numerically under the assumption of constant T for each measurement of $R(t)$. We show these integrations of $G(R(t))$ in Fig. 8 as a solid line with circles, shifted in the vertical direction (i.e., for arbitrary $T = T_0$) for clarity since our interest is in scaling behavior. The function captures qualitatively the way that the ring in the experiment slowed down relative to a power law of time as the radius of the ring approached zero. Indeed, in the last hour (54 000 cycles) of the experiment, both the

incompressible model and the data showed a change of only a few percent (6–8 %) in the ring radius.

Though the scaling arguments embodied in Eqs. (16) and (20) capture the essential features of the development of the heap, a granular bed is not incompressible, as we assumed until now. Since the net volume of a granular bed can change due to changes in the way the beads are packed within the bed, a heap can grow as a consequence of a decrease in its depth-averaged mass density, $\bar{\rho}(r, t)$. To see this, consider that Eq. (17) is an incompressible simplification of

$$\frac{\partial}{\partial t}(\bar{\rho}h) = -\frac{1}{r} \frac{\partial}{\partial r}(r\bar{\rho}uh) \quad (21)$$

for a compressible material. We introduce a radius, r_0 , within which the radial flux is identically zero. In the incompressible analysis, the radial flux approaches zero asymptotically toward small r , but in the available data this behavior cannot be distinguished from one where the flux is zero within r_0 . We find that within this radius the heap height changes due to changes in the mass density alone, and not to radial flux, since $dh = -(h/\bar{\rho})d\bar{\rho}$ within this region. In the absence of radial flux, the observed change in height of the bed corresponds to a change in density of 10–20 %.

By integrating the profiles in Fig. 6 we observed qualitatively that the volume of the trough around the heap balanced the volume of the heap itself, but with large enough uncertainty that it was impossible to establish whether the mass density of the material changed either in time or across the heap. Further experiments are needed to determine the relative contributions from the radial flux and from the changes in mass density.

V. CONCLUSIONS

The arguments and predictions outlined above are consistent with the essential features of the onset of sediment transport and the subsequent development of the heap, while also calling attention to the importance of motions internal to the heap. At the coarse-grained scale, these motions include changes in the mass density of the bed and the depth of penetration of the granular deformation. At the scale of grains, the motions include creep, jamming, and ratcheting, and an important thrust of future work will be to explore the limitations of the continuum models employed here. While other mechanisms may ultimately fully explain the response of the bed to the fluid stresses we applied to it, we observed that sediment motion due to pressure gradients and a subsequent viscous deformation agree with the data as hypothesized by Johnson [14] in their experiments involving irregular oscillations. Future studies could evaluate these internal motions quantitatively as well as the extent to which permeability gradients change the presented results, the relationships between the heap’s dimensions and the grain size, and the relationships between the heap’s shape distributions and plate geometry.

ACKNOWLEDGMENTS

This research was supported in part by the U.S. Office of Naval Research, Global, London (N62909-17-1-2048). This

material is based upon work supported by the National Science Foundation under Grant No. CBET-2035303.

APPENDIX

The Laplace equation governs the pressure distribution within the bed:

$$\frac{\partial^2 p'}{\partial x^2} + \frac{\partial^2 p'}{\partial y^2} = 0, \quad (\text{A1})$$

with the condition at surface of the bed

$$p'(r, 0, t) = -\frac{\rho A}{4H} \omega^2 \sin(\omega t)(r^2 - W^2). \quad (\text{A2})$$

If we make both r and z dimensionless by W then, within the bed, $0 < \hat{r} < 1$ and $\hat{z} < 0$, the solution of Eq. (A1) is

$$p'(\hat{r}, \hat{z}, t) = \sum_{n=1}^{\infty} a_n e^{\lambda_n \hat{z}} J_0(\hat{\lambda}_n \hat{r}) \omega^2 \sin(\omega t),$$

where the assumption that $p'(1, 0, t) = 0$ gives the λ_n as the values at which $J_0(\hat{\lambda}_n) = 0$. Then, the a_n are determined by

$$\frac{\rho A}{4H} W^2 (1 - \hat{r}^2) = \sum_{n=1}^{\infty} a_n J_0(\hat{\lambda}_n \hat{r}),$$

with

$$\int_0^1 [J_0(\hat{\lambda}_n \hat{r})]^2 \hat{r} d\hat{r} = \frac{1}{2} [J_1(\hat{\lambda}_n \hat{r})]^2$$

and

$$a_n = \frac{\rho A}{2H} \frac{W^2}{[J_1(\hat{\lambda}_n)]^2} \int_0^1 (1 - \hat{r}^2) J_0(\hat{\lambda}_n \hat{r}) \hat{r} d\hat{r}.$$

For example, $J_0(\hat{\lambda}_1) = 0$ when $\hat{\lambda}_1 \doteq 2.41$. Then, $J_1(2.41) \doteq 0.52$, $J_2(2.41) \doteq 0.43$, and $J_3(2.41) \doteq 0.20$. So,

$$\int_0^1 J_0(\hat{\lambda}_n \hat{r}) \hat{r} d\hat{r} = \frac{1}{\hat{\lambda}_n} J_1(\hat{\lambda}_n)$$

and

$$\int_0^1 J_0(\hat{\lambda}_n \hat{r}) \hat{r}^3 d\hat{r} = \frac{1}{\hat{\lambda}_n^2} [2J_2(\hat{\lambda}_n) - \hat{\lambda}_n J_3(\hat{\lambda}_n)].$$

At lowest order,

$$a_1 = \frac{\rho A}{2H} \frac{W^2}{[J_1(\hat{\lambda}_1)]^2} \frac{1}{\hat{\lambda}_1} \left\{ J_1(\hat{\lambda}_1) - \frac{1}{\hat{\lambda}_1} [2J_2(\hat{\lambda}_1) - \hat{\lambda}_1 J_3(\hat{\lambda}_1)] \right\}.$$

Then,

$$a_1 = 0.28 \rho \frac{A}{H} W^2 \quad (\text{A3})$$

and, finally, at lowest order in the Fourier series, the perturbation to the pressure in the porous bed is

$$p'(\hat{r}, \hat{z}, t) = 0.28 \rho \frac{A}{H} (\omega W)^2 \times e^{2.41 \hat{z}} J_0(2.41 \hat{r}) \sin \omega t. \quad (\text{A4})$$

-
- [1] F. Charru, B. Andreotti, and P. Claudin, *Annu. Rev. Fluid Mech.* **45**, 469 (2013).
- [2] R. A. Bagnold and G. I. Taylor, *Proc. R. Soc. London A* **157**, 594 (1936).
- [3] F. Francken, S. Wartel, R. Parker, and E. Taverniers, *Geo-Mar. Lett.* **24**, 14 (2004).
- [4] P. Claudin and B. Andreotti, *Earth Planet. Sci. Lett.* **252**, 30 (2006).
- [5] S. Diniega, M. Kreslavsky, J. Radebaugh, S. Silvestro, M. Telfer, and D. Tirsch, *Aeolian Res.* **26**, 5 (2017).
- [6] D. A. Barone, K. K. McKenna, and S. C. Farrell, *Shore Beach* **82**, 13 (2014).
- [7] D. B. Loope, J. A. Mason, and L. Dingus, *J. Geol.* **107**, 707 (1999).
- [8] G. Masselink, L. Cointre, J. Williams, R. Gehrels, and W. Blake, *Mar. Geol.* **262**, 82 (2009).
- [9] S. Dey, *Fluvial Hydrodynamics: Hydrodynamic and Sediment Transport Phenomena* (Springer, Berlin, 2014).
- [10] B. Yohannes and K. M. Hill, *Phys. Rev. E* **82**, 061301 (2010).
- [11] Y. Fan and K. M. Hill, *Phys. Rev. Lett.* **106**, 218301 (2011).
- [12] G. Juarez, P. Chen, and R. M. Lueptow, *New J. Phys.* **13**, 053055 (2011).
- [13] H. K. Pak and R. P. Behringer, *Phys. Rev. Lett.* **71**, 1832 (1993).
- [14] B. A. Johnson, Ph.D. thesis, Cornell University, 2016.
- [15] B. A. Johnson and E. A. Cowen, *J. Fluid Mech.* **894**, A8 (2020).
- [16] Marc Lämmel, A. Meiwald, H. Tsoar, I. Katra, and K. Kroy, *Nat. Phys.* **14**, 759 (2018).
- [17] F. Engelund and J. Fredsoe, *Annu. Rev. Fluid Mech.* **14**, 13 (1982).
- [18] J. B. Southard, *Annu. Rev. Earth Planet. Sci.* **19**, 423 (1991).
- [19] M. Sumer, *Liquefaction Around Marine Structures* (World Scientific, Singapore, 2014).
- [20] P. L. Liu, Y. S. Park, and J. L. Lara, *J. Fluid Mech.* **586**, 323 (2007).
- [21] G. A. Rivera-Rosario, P. J. Diamesis, and J. T. Jenkins, *J. Geophys. Res. Oceans* **122**, 5468 (2017).
- [22] A. Shields, *Mitt. Preuss. Vers. Wasser. Schiff.* **26**, 524 (1936).
- [23] H. A. Einstein and E. S. A. El-Samni, *Rev. Mod. Phys.* **21**, 520 (1949).
- [24] A. M. Mollinger and F. T. Nieuwstadt, *J. Fluid Mech.* **316**, 285 (1996).
- [25] D. L. Foster, A. J. Bowen, R. A. Holman, and P. Nattoo, *J. Geophys. Res.* **111**, 1 (2006).
- [26] J. F. Sleath, *Cont. Shelf Res.* **19**, 1643 (1999).
- [27] E. A. Cowen, I. M. Sou, P. L.-F. Liu, and B. Raubenheimer, *J. Eng. Mech.* **129**, 1119 (2003).
- [28] W. Gong, P. A. Taylor, and A. Dörnbrack, *J. Fluid Mech.* **312**, 1 (1996).

- [29] R. A. Musa, S. Takarrouht, M. Y. Louge, J. Xu, and M. E. Berberich, *J. Geophys. Res. Earth Surf.* **119**, 2574 (2014).
- [30] M. Y. Louge, A. Valance, A. Ould el Moctar, and P. Dupont, *J. Geophys. Res.* **115**, F02002 (2010).
- [31] L. La Razione, K. Laurent, J. T. Jenkins, and G. P. Bewley, *Phys. Rev. Lett.* **123**, 058501 (2019).
- [32] C. P. Ortiz, K. E. Daniels, and R. Riehn, *Phys. Rev. E* **90**, 022304 (2014).
- [33] W. Losert, D. G. W. Cooper, J. Delour, A. Kudrolli, and J. P. Gollub, *Chaos* **9**, 682 (1999).
- [34] W. S. Merritt, R. A. Letcher, and A. J. Jakeman, *Environ. Modell. Softw.* **18**, 761 (2003).
- [35] L. B. H. May, L. A. Golick, K. C. Phillips, M. Shearer, and K. E. Daniels, *Phys. Rev. E* **81**, 051301 (2010).
- [36] L. Bocquet, W. Losert, D. Schalk, T. C. Lubensky, and J. P. Gollub, *Phys. Rev. E* **65**, 011307 (2001).
- [37] S. Li and D. L. Henann, *Phys. Rev. E* **102**, 022908 (2020).
- [38] A. Thoesen, T. McBryan, D. Mick, M. Green, J. Martia, and H. Marvi, *Phys. Rev. E* **102**, 032902 (2020).
- [39] G. K. Batchelor, *An Introduction to Fluid Dynamics* (Cambridge University Press, Cambridge, UK, 1967).
- [40] H. Darcy, *Les fontaines publiques de la ville de Dijon* (Dalmont, Paris, 1856).
- [41] G. D. Scott and D. M. Kilgour, *J. Phys. D: Appl. Phys.* **2**, 863 (1969).
- [42] M. Houssais, C. P. Ortiz, D. J. Durian, and D. J. Jerolmack, *Nat. Commun.* **6**, 6527 (2015).
- [43] P. Marchal, C. Hanotin, L. J. Michot, and S. Kiesgen de Richter, *Phys. Rev. E* **88**, 012207 (2013).
- [44] C. Hanotin, S. Kiesgen de Richter, P. Marchal, L. J. Michot, and C. Baravian, *Phys. Rev. Lett.* **108**, 198301 (2012).
- [45] C. Hanotin, P. Marchal, L. J. Michot, C. Baravian, and S. Kiesgen De Richter, *Soft Matter* **9**, 9352 (2013).
- [46] M. van Hecke, *C. R. Phys.* **16**, 37 (2015).
- [47] K. Wu, V. Francia, and M.-O. Coppens, *Powder Technol.* **365**, 172 (2020).
- [48] S. A. Elaskar, L. A. Godoy, D. D. Gray, and J. M. Stiles, *Int. J. Solids Struct.* **37**, 2185 (2000).
- [49] G. I. Barenblatt and Y. B. Zeldovich, *Russ. Math. Surv.* **26**, 45 (1971).
- [50] E. Buckingham, *Phys. Rev.* **4**, 345 (1914).
- [51] G. Bewley and K. Sreenivasan, *J. Low Temp. Phys.* **156**, 84 (2009).
- [52] R. Soulsby and R. Whitehouse, in *Proceedings of the Pacific Coasts and Ports '97*, Vol. 1 (University of Canterbury, Christchurch, New Zealand, 1997), p. 145.